Iron Coordination in Photosystem II: Interaction between Bicarbonate and the Q_B Pocket Studied by Fourier Transform Infrared Spectroscopy†

Catherine Berthomieu‡ and Rainer Hienerwadel*,§

CEA/Saclay, Section de Bioénergétique Bat. 532, 91 191 Gif-sur-Yvette, Cedex, France

Received September 22, 2000; Revised Manuscript Received January 9, 2001

ABSTRACT: The non heme iron environment of photosystem II is studied by light-induced infrared spectroscopy. A conclusion of previous work [Hienerwadel, R., and Berthomieu, C. (1995) *Biochemistry 34*, 16288−16297] is that bicarbonate is a bidendate ligand of the reduced iron and a monodentate ligand in the Fe^{3+} state. In this work, the effects of bicarbonate replacement with lactate, glycolate, and glyoxylate, and of *o*-phenanthroline binding are investigated to determine the specific interactions of bicarbonate with the protein. Fe^{2+}/Fe^{3+} FTIR spectra recorded with ^{12}C- and $^{13}C_1$-labeled lactate indicate that lactate displaces bicarbonate by direct binding to the iron through one carboxylate oxygen and the hydroxyl group in both the Fe^{2+} and Fe^{3+} states. This different binding mode with respect to bicarbonate could explain the lower midpoint of the iron couple observed in the presence of this anion [Deligiannakis, Y., Petrouleas, V., and Diner, B. A. (1994) *Biochim. Biophys. Acta 1188*, 260−270]. In agreement with the −60 mV/pH unit dependence of the iron midpoint potential in the presence of bicarbonate, the proton release upon iron oxidation by photosystem II is directly measured to 0.95 ± 0.05 by the comparison of infrared signals of phosphate buffer and ferrocyanide modes. This accurate method may be applied to the study of other redox reactions in proteins. The pH dependence of the iron couple is proposed to reflect the deprotonation of D1His215, a putative iron ligand located at the Q_B pocket, since the signal at 1094 cm^{-1} assigned to the ν(C−N) mode of a histidinate ligand in the Fe^{3+} state is not observed in the presence of *o*-phenanthroline. Specific regulation of the pK_a of D1His215 by bicarbonate is inferred from the absence of the band at 1094 cm^{-1} in Fe^{2+}/Fe^{3+} spectra recorded with glycolate, glyoxylate, or lactate. A broad positive continuum, maximum at ≈2550 cm^{-1}, observed in the presence of bicarbonate, but absent with *o*-phenanthroline or lactate, glycolate, and glyoxylate, indicates a hydrogen bond network from the non heme iron toward the Q_B pocket involving bicarbonate and His D1−215. Proton release of about 1, measured upon iron oxidation at pH 6 with the latter anions, points to a proton release mechanism different from that involved in the presence of bicarbonate.

The primary steps of light to chemical energy conversion in photosystem II (PS II)[1] of plants and cyanobacteria, as in the photosynthetic reaction center (RC) of purple bacteria, result in the reduction and protonation of quinone Q_B to the quinol form Q_BH_2. In both systems, light absorption at a (bacterio)chlorophyll cofactor leads to the transient reduction of a primary electron acceptor quinone, Q_A, which transfers its electron to the secondary acceptor Q_B. The Q_B binding pocket controls the double reduction of this quinone by two sequential steps and its protonation to the quinol, which diffuses in the membrane.

The electron-transfer steps involving the quinones are comparable in PS II and bacterial RC [reviewed in (*1*)]. Structural analogies between the two proteins at the quinone binding sites are evidenced by sequence homology between the main polypeptides of PS II (D1 and D2) and bacterial RC (L and M) and by models established for PS II from the known structure of the bacterial RC (*2*−*16*). In both proteins, a non heme iron is located between the quinones, coordinated in a similar distorted octahedral arrangement (*17*). Four histidines and a bidentate glutamate (M232) provide the iron ligands in bacterial RC (*4*−*6*, *9*−*13*, *18*). Four homologous histidines are found in D1 (D1−215, D1−272) and D2 (D2−215, D2−269) (*3*, *6*). There is, however, no equivalent of Glu M232 in PS II (*3*, *6*, *14*−*16*). Instead, EPR, Mössbauer, and fluorescence yield relaxation measurements have shown that bicarbonate competes with nitrogen oxide or cyanide bound to Fe^{2+}, supporting that bicarbonate is a fully

† Part of this work was supported by EC Fellowship ERB40016T-933365 to R.H.

* Corresponding author. FAX: 00 33 4 91 82 94 12; Tel: 00 33 4 91 82 94 11; E. mail: rhiener@luminy.univ-mrs.fr.

‡ Present address: CEA/Cadarache, DEVM/LBC, Bat. 156, 13108 Saint Paul-lez-Durance, France. E-mail: cberthomieu@cea.fr.

§ Present address: Laboratoire de Biophysique des Transporteurs d'Electron, Université d' Aix-Marseille II, Case 901, 163 Avenue de Luminy, 13288 Marseille Cedex 9, France.

[1] Abbreviations: PS II, photosystem II; RC, reaction center; Q_A (Q_B), primary (secondary) electron acceptor quinone; Fe^{2+} (Fe^{3+}), non heme iron in its reduced (oxidized) state; D1 (L) and D2 (M), polypeptides constituting the anchoring site of the main cofactors for PS II (bacterial RC); $E_m(Fe^{3+}/Fe^{2+})$, midpoint potentiel of the non heme iron redox couple; Tris, tris(hydroxymethyl)aminomethane; MES, 2-(*N*-morpholino)ethanesulfonic acid; HEPES, *N*-(2-hydroxyethyl)piperazine-*N*′-2-ethanesulfonic acid; atrazine, 2-chloro-4-(ethylamino)-6-isopropylamino-*s*-triazine; terbutryn, 2-*tert*-butylamino-4-(ethylamino)-6-methylthio-*s*-triazine; DCMU or diuron, 3-(3,4-dichlorophenyl)-1,1-dimethylurea; FTIR, Fourier transform infrared; IR, infrared; ν_{as} (ν_s), asymmetric (symmetric) stretching vibration; δ, bending vibration; EPR, electron paramagnetic resonance; au, absorption unit.

10.1021/bi002236l CCC: $20.00
Published on Web 03/08/2001

dissociable ligand of the iron (*19*−*21*). The infrared modes of bicarbonate strongly indicate that bicarbonate is a bidentate ligand of Fe^{2+} in PS II (*22*). This result together with the analysis of the Fe^{2+}−NO EPR signal in oriented membranes (*23*) points to a location of bicarbonate in PS II homologous to that of the Glu M232 side chain in bacterial RC.

Bicarbonate is responsible for some specific properties of the quinone-iron electron acceptor side in PS II [reviewed in (*1, 24, 25*)]. It has a strong influence on the electron-transfer rates between the quinones, the mechanisms of Q_B^{2-} protonation, and the binding affinity of herbicides (*26*−*30*). It also determines the midpoint potential of the iron [$E_{m,7}$-(Fe^{3+}/Fe^{2+}) = 400 mV] and its pH dependence, −60 mV/pH unit between pH 5.5 and pH 8, which indicates deprotonation of a group(s) in this pH range upon iron oxidation (*26, 29, 31*−*33*). According to FTIR data, the bicarbonate ligand does not deprotonate but probably becomes a monodentate ligand to Fe^{3+} (*22*). It may regulate the pH dependence of the iron midpoint potential by defining the pK_a of protonatable group(s) since bicarbonate exchange by other carboxylate anions alters both the iron midpoint potential and its pH dependence (*34*). In particular, formate and oxalate raise $E_m(Fe^{3+}/Fe^{2+})$, while glycolate, glyoxylate, or lactate lowers $E_m(Fe^{3+}/Fe^{2+})$ (*34*).

The identification of the group(s) sensitive to the iron redox state and the analysis of bicarbonate interactions within the protein will provide information on the mechanism of regulation by bicarbonate of the electron-transfer rate between Q_A^- and Q_B and of proton-transfer reactions stabilizing the semiquinone or participating in the formation of the quinol (*26*−*28*). In a previous FTIR study, we assigned two ^{15}N-sensitive signals to histidine ligands of the iron, one of which, at 1094 cm^{-1}, was proposed to correspond to a histidinate in the Fe^{3+} state (*22*). In the present paper, we analyze the effect of bicarbonate replacement by glycolate, lactate, and glyoxylate on the Fe^{2+}/Fe^{3+} FTIR spectrum to probe the amino acids specifically influenced by bicarbonate, and to determine the binding mode of these carboxylate anions. A preliminary analysis of bicarbonate replacement by glycolate was reported previously (*35*). Since the oxidation state of the iron modifies the binding affinity of various herbicides toward the Q_B pocket, and since the EPR spectrum of the oxidized iron is sensitive to the presence of exogenous quinones or herbicides in the Q_B pocket (*29, 36*−*38*), the interactions between bicarbonate and the Q_B binding site are studied by comparison of Fe^{2+}/Fe^{3+} spectra obtained in the presence or absence of *o*-phenanthroline. We notably focus on the sensitivity of the histidinate signal at 1094 cm^{-1} to these conditions. A quantification of proton release by PS II upon non heme iron oxidation is shown for the first time, using the quantitative determination of proton uptake/release by phosphate buffer.

MATERIALS AND METHODS

Photosystem II enriched membranes were prepared from spinach and subsequently Mn-depleted by Tris treatment, as previously described (*22*). Bicarbonate exchange by glycolate, glyoxylate, and lactate was performed essentially as described in (*34*). The samples were incubated at pH 6 in MES or phosphate buffer (50 mM) with 50 mM of the carboxylate salt for 1−5 h on ice. The buffers were flushed with nitrogen gas to minimize the presence of bicarbonate. The FTIR sample consisted of a pellet of PS II enriched membranes sandwiched between two CaF_2 windows. The samples were prepared as described in (*39*).

FTIR difference spectra were recorded on a Bruker 88 SX spectrometer equipped with a MCT-A detector and a sample holder maintained at 4 °C. All spectra were recorded with 4 cm^{-1} resolution. Illumination of the sample was performed either by the broad band emission of sulforhodamine 101 pumped by the 10 ns pulse of a frequency doubled Nd:YAG laser (Quantel YG 780-50) or by 0.6 s illumination with a 680 nm laser diode (20 mW). Fe^{2+}/Fe^{3+} FTIR spectra were obtained by computing the difference between the infrared absorption spectra of the sample obtained after (40 scans, 7 s duration) and before (64 scans, 11 s duration) illumination. For experiments performed in the presence of lactate, glycolate, and glyoxylate, an equimolar solution of ferricyanide and ferrocyanide was used as the electron donor/acceptor system, and the recording time after illumination was shortened to 5 s. Analysis of PS II with formate, oxalate, or DCMU was hindered by the impossibility of oxidizing the iron by ferricyanide and photoreducing it reversibly in these conditions. Measurements were cycled up to 24 h, allowing the sample to dark-adapt for 80 s between successive illuminations. Spectra obtained with 2−8 samples were averaged.

To measure the IR absorption of phosphate buffer, 50 mM stock solutions of KH_2PO_4 and K_2HPO_4 were mixed to the intended pH. The calibration of phosphate and ferrocyanide signals was obtained by quantitative absorbance measurements with a liquid transmission cell (Harris) of fixed path length (18 μm). All measurements were performed at room temperature.

The effect of Cu−lactate interaction on the IR modes of lactate was studied by comparing the FTIR spectra of sodium lactate solutions (obtained by neutralization of lactic acid, 10 M, to pH 8 with NaOH) in the presence of increasing concentrations of $CuCl_2$. The spectrum in Figure 2D (thin line) is the difference between the spectrum obtained with lactate and 2 M $CuCl_2$ solution *minus* that obtained with lactate and 0.2 M $CuCl_2$ solution. The insoluble powder of the $Fe(lactate)_2(H_2O)_3$ complex (Prolabo) was maintained between two CaF_2 windows by addition of water. The water IR absorption was then subtracted to obtain the FTIR spectrum shown in Figure 2D (thick line).

RESULTS

Light-induced Fe^{2+}/Fe^{3+} FTIR difference spectra without contributions from the donor side of PS II were previously reported using Tris-washed or hydroxylamine-treated PS II enriched membranes of spinach in the presence of ferricyanide (*22*, *39*, *40*; see also *41*). Figure 1 compares Fe^{2+}/Fe^{3+} spectra obtained in the presence of bicarbonate (Figure 1A), glycolate (1B, *35*), glyoxylate (1C), and ^{12}C- or $^{13}C_1$-lactate (1D, thick and thin lines, respectively). The spectra were recorded at pH 6 to avoid contributions of PS II centers (≈15%) which show a different rhombic Fe^{3+} EPR signal at $g = 4.3$ at pH ≥7 in the presence of these anions (*34*). In these spectra, positive signals correspond to the Fe^{2+} state, negative ones to the Fe^{3+} state. IR modes of the iron ligands contribute as well as modes from all amino acid side chains

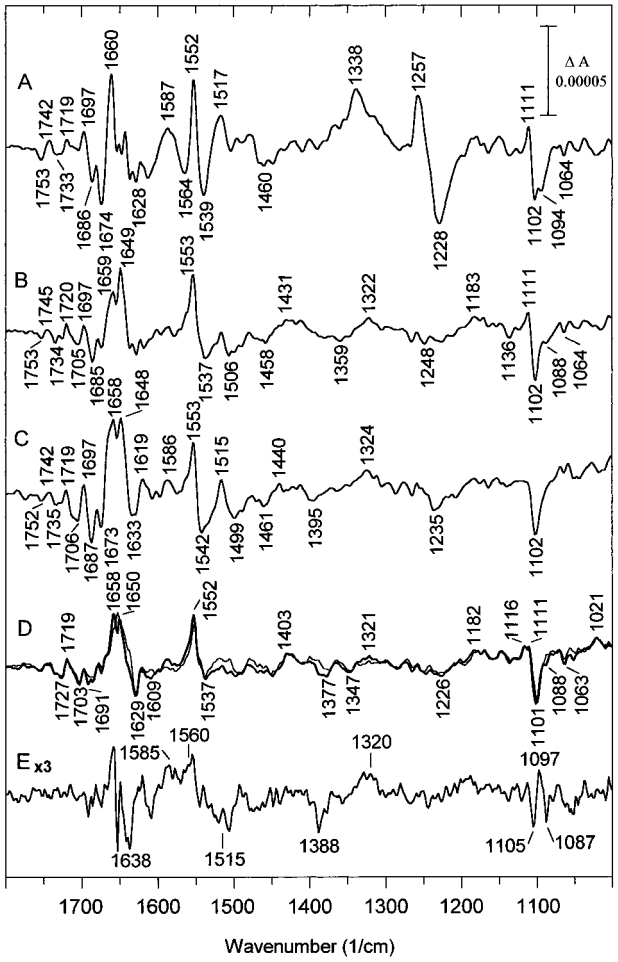

FIGURE 1: Comparison of Fe^{2+}/Fe^{3+} FTIR difference spectra recorded with MES buffer at pH 6 (A) in the presence of 50 mM bicarbonate, (B) 50 mM glycolate, (C) 50 mM glyoxylate, and (D) 50 mM lactate (thick line) or $^{13}C_1$-lactate (thin line); (E) ^{12}C-*minus*-$^{13}C_1$-lactate difference spectrum obtained by subtraction of spectra in (D). A total of ≈500 000 scans per spectrum, 4 °C.

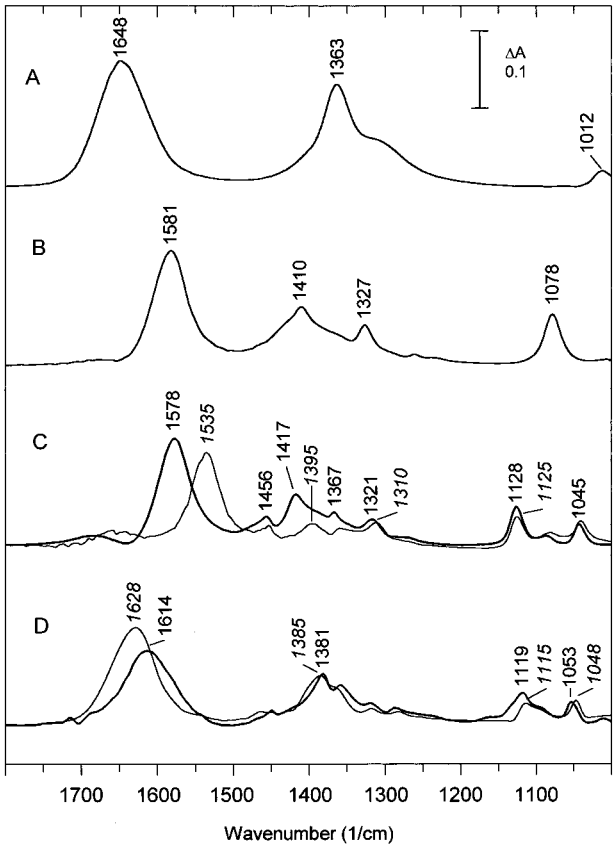

FIGURE 2: Absorption spectra of (A) bicarbonate, (B) glycolate, and (C) ^{12}C-lactate (thick line) and $^{13}C_1$-lactate (thin line). A 1 M concentration of the sodium salt was used in NaOH−water solution. The absorption spectra were first calibrated to the same absorption of the water Fermi resonance at ≈2130 cm^{-1}. Then the absorption of the NaOH solution was subtracted. A total of 400 scans/spectrum, room temperature. (D) Absorption spectra of $Fe(lactate)_2(H_2O)_3$ (thick line) and Cu−lactate complexes (thin line).

or backbones that reorganize upon iron reduction. The Fe^{2+}/Fe^{3+} spectrum recorded with bicarbonate at pH 6 is identical to that at pH 8 although smaller signals are obtained. This is due to the higher midpoint potential of the Fe^{3+}/Fe^{2+} couple at this pH which results in a lower amount of iron oxidizable by ferricyanide. In this spectrum (Figure 1A), the strong signals at 1257, 1338, and 1228 cm^{-1} were assigned to bicarbonate δ(COH) (Fe^{2+} state), ν_s(CO) (Fe^{2+} state), and ν_s(CO) (Fe^{3+} state) IR modes. Above 1500 cm^{-1}, using ^{13}C-bicarbonate, we identified the ν_{as}(CO) mode of bicarbonate at 1530 ± 10 cm^{-1} in the Fe^{2+} state and at 1658 ± 20 cm^{-1} in the Fe^{3+} state (*22*). Signals at 1674/1660 and 1552/1539 cm^{-1} were attributed to slight conformational changes of one or a few peptide bonds, and signals at 1111/1102 and 1094 cm^{-1} were assigned to side chain modes of histidine ligands of the iron (*22*).

Substitution of bicarbonate by other carboxylate anions causes the complete disappearance of the bicarbonate signals at 1338, 1257, and 1228 cm^{-1}. In contrast, no significant signals of the carboxylate anions can be identified at first. Comparison of the IR absorption spectra of equimolar solutions of bicarbonate (Figure 2A), glycolate (2B), and lactate (2C, thick line) shows the strong difference between extinction coefficients of the ν_s(CO) mode of bicarbonate and glycolate or lactate, and explains why the ν_s(CO) modes of the latter anions do not clearly show up in the Fe^{2+}/Fe^{3+} spectra.

The overall shape of the Fe^{2+}/Fe^{3+} spectra in Figure 1B−D is conserved, suggesting that these anions, which differ only by the substituent at the C_2 carbon (-H_2COH, -HCO, and -CH_3COH, respectively), bind in PS II in a similar way. Binding of these anions also alters the Fe^{3+} EPR spectrum in a similar way (*34*), corresponding to a slight increase in rhombicity of the iron environment. Since there is no direct evidence that the anions bind to the iron (see, however, *42*, *43*), we identified the lactate IR modes in the Fe^{2+}/Fe^{3+} spectrum by specific labeling and compared them to those of lactate in solution or in Cu− and Fe−lactate complexes.

The Fe^{2+}/Fe^{3+} spectra recorded in the presence of ^{12}C-lactate and lactate ^{13}C-labeled at the C_1 carbon ($^{13}C_1$-lactate) are shown in Figure 1D (thick and thin lines, respectively). The ^{12}C -*minus*-$^{13}C_1$ difference spectrum presented in Figure 1E shows up solely modes of lactate sensitive to $^{13}C_1$-labeling, i.e., without spectral contribution of the protein. In this spectrum, negative signals are observed at 1638, 1515, and 1388 cm^{-1} and positive ones at 1585−1560 and 1320 cm^{-1}. A differential signal is also observed at 1105/1097/1087 cm^{-1}.

In solution, the ν_{as}(CO) and ν_s(CO) modes of lactate observed at 1578 and 1417 cm^{-1} are downshifted by 43 and

22 cm^{-1} upon $^{13}C_1$-labeling, respectively (Figure 2C). The intensity of the ν_s(CO) mode of $^{13}C_1$-lactate is significantly smaller than that of ^{12}C-lactate. Other lactate modes are of lower intensity, except for the stretching mode of the alcohol group in C_2, ν_{AL}(C−OH), at 1128 cm^{-1} (*44*, *45*) downshifted by ≈3 cm^{-1} upon $^{13}C_1$-labeling (Figure 2C).

For PS II, positive bands at 1560 and 1320 cm^{-1} in Figure 1E are assigned to the ν_{as} and ν_s(CO) modes of ^{12}C-lactate in the Fe^{2+} state. The negative signal at ≈1515 cm^{-1} is assigned to the corresponding ν_{as}(CO) mode of $^{13}C_1$-lactate. The downshift by ≈45 cm^{-1} upon $^{13}C_1$-lactate labeling is similar to that observed in solution. The ν_s(CO) mode of $^{13}C_1$-lactate expected around 1300 cm^{-1} is under the detection limit of the experiment (see above). In the Fe^{3+} state, negative bands at 1638 and 1388 cm^{-1} are assigned to the ν_{as}(CO) and ν_s(CO) modes of ^{12}C-lactate and the positive signal at 1585 cm^{-1} to the ν_{as}(CO) mode of $^{13}C_1$-lactate (downshifted by 53 cm^{-1}). The differential signal at 1105/1097/1087 cm^{-1} in Figure 1E is assigned to the ν_{AL}(C−OH) mode. This signal results from modes of ^{12}C-lactate slightly downshifted upon $^{13}C_1$ labeling both in the Fe^{2+} and in the Fe^{3+} state.

Despite overall similarities, the frequencies of lactate IR modes in PS II differ from those observed in solution. They are closer to those observed in the IR spectra of Cu^{2+}−lactate and $Fe^{2+}(lactate)_2(H_2O)_3$ complexes (Figure 2D, thin and thick lines, respectively). For these complexes, the ν_{as}(CO) and ν_s(CO) modes of lactate are observed at 1614−1628 and 1381−1385 cm^{-1}, i.e., up- and downshifted by 36−50 and 32−36 cm^{-1}, respectively, as compared to the frequencies of lactate in solution. Thus, the frequency differences $\nu_{as} - \nu_s$(CO) observed for the Fe− and Cu−lactate complexes (233 and 243 cm^{-1}, respectively) are larger than that observed for lactate in solution (161 cm^{-1}), where lactate associates through the hydroxyl groups, leaving the carboxylate free from intermolecular interactions (*44*). As previously discussed for bicarbonate (*22*), the large $\nu_{as} - \nu_s$(CO) frequency difference indicates that the carboxylate of lactate provides a monodentate metal ligand in the Cu− and Fe−lactate complexes (*46*). The ν_{AL}(C−OH) mode, which contributes as a broad band at 1119−1095 cm^{-1} in the Cu and Fe complexes, is significantly downshifted as compared to that of lactate in solution (−9 to −23 cm^{-1}). This low frequency is correlated with metal chelation by the hydroxyl group in C_2 (*45*). A downshift of 15−19 cm^{-1} of the glycolate ν_{AL}(C−OH) mode was also reported for several glycolate−divalent metal complexes, where glycolate binds both through the carboxylate and through the hydroxyl groups (*47*, *48*).

In PS II, both in the Fe^{2+} and in the Fe^{3+} states, the $\nu_{as} - \nu_s$(CO) frequency difference for the lactate IR modes (240 and 250 cm^{-1}, respectively) is close to that observed for the Fe− and Cu−lactate complexes. The ν_{AL}(C−OH) mode of lactate appears at a low frequency (≈1105−1087 cm^{-1}) close to that of the metal−lactate complexes. We conclude that lactate is a bidentate ligand of the iron, bound through its carboxylate and hydroxyl groups, both in the Fe^{2+} and in the Fe^{3+} states. In the Fe^{2+} state, however, the frequencies of the ν_{as}(CO) and ν_s(CO) modes are lower by ≈60 cm^{-1} than those observed for the metal−lactate complexes. This might indicate the implication of the carboxylate in strong hydrogen bonding interactions with neighboring amino acids which weaken upon iron oxidation.

Bicarbonate exchange by the other anions affects several IR modes from the protein backbone or amino acid side chains in the Fe^{2+}/Fe^{3+} spectrum. The large signal at 1660 cm^{-1} in Figure 1A, attributed to the ν(C═O) vibration of a peptide group, appears to split into two signals of similar intensities pointing at 1658−1659 and 1648−1650 cm^{-1} for glycolate, glyoxylate, and lactate. A differential signal at 1697/1685−1687 cm^{-1} in Figure 1A−C is absent in the Fe^{2+}/Fe^{3+} spectrum recorded in the presence of lactate (Figure 1D). This signal is best interpreted as a ν(C═O) mode, either from the peptide backbone or from glutamine or asparagine side chains, since it is downshifted only by 1−2 cm^{-1} upon ^{15}N labeling (*22*). This specific effect points to a conformational change induced by the methyl group of lactate. At 1700−1760 cm^{-1}, a straightforward interpretation of the small differences between spectra of Figure 1 is not possible since both Asp or Glu side chains and the C═O ester groups from cofactors at longer distances may contribute. Long-range electrostatic interactions have been recently demonstrated for the Q_A^-/Q_A FTIR spectrum of *Rb. sphaeroides* (*49*).

Above 2200 cm^{-1}, a small broad positive continuum band is observed in the Fe^{2+}/Fe^{3+} spectrum recorded in the presence of bicarbonate, maximum at ≈2550 cm^{-1} in H_2O (Figure 4b), and downshifted to ≈2050 cm^{-1} in ^2H_2O (not shown). Similar broad positive bands in this spectral range, downshifted by about 500 cm^{-1} in ^2H_2O, were also detected in the Q_A^-/Q_A and Q_B^-/Q_B FTIR spectra of bacterial RC and interpreted as a net increase in proton concentration within a large web of polarized hydrogen bonds involving cofactors, amino acid residues, and structured water molecules (*50*, *51*). This broad continuum is not present in the Fe^{2+}/Fe^{3+} spectra recorded in the presence of glycolate or lactate (Figure 4c,d, respectively).

In the spectra recorded with glycolate, glyoxylate, and lactate (Figure 1B−D), only one thin negative band appears at 1102 cm^{-1}, which is assigned to the side chain of histidine ligand(s) of the iron (*22*). The IR signal at 1094 cm^{-1} in Figure 1A proposed to account for a histidinate ligand of Fe^{3+} is absent. Binding of lactate, glyoxylate, and glycolate thus affects one histidine ligand of the iron. These ions either interact directly with the histidine or influence the pH dependence of this signal.

Effect of o-Phenanthroline Binding to the Q_B Pocket. Figure 3A compares the Fe^{2+}/Fe^{3+} FTIR spectra recorded in the presence (thick line) or absence (thin line) of *o*-phenanthroline at pH 7. *o*-Phenanthroline binding affects both IR modes of the protein and bicarbonate. The bicarbonate modes have been identified by comparing Fe^{2+}/Fe^{3+} spectra recorded in the presence of *o*-phenanthroline and ^{12}C-bicarbonate (thin line) or ^{13}C-bicarbonate (thick line) (Figure 3B). The ^{12}C-*minus*-^{13}C-bicarbonate difference spectrum in Figure 3C (thick line), computed from spectra of Figure 3B, is superimposed to the equivalent ^{12}C-*minus*-^{13}C spectrum obtained with PS II without *o*-phenanthroline (thin line, *22*). In the Fe^{2+} state, bicarbonate ν_{as}(CO) and ν_s(CO) modes at 1530 and 1334 cm^{-1}, downshifted to 1495 and 1305 cm^{-1}, respectively, upon ^{13}C labeling, are almost unaffected by *o*-phenanthroline binding. In contrast, bicarbonate modes are hardly distinct in the presence of *o*-phenanthroline in the Fe^{3+} state (Figure 3C, thick line). The ν_s(CO) mode contributes now as a small broad signal maximum at 1246 cm^{-1} which

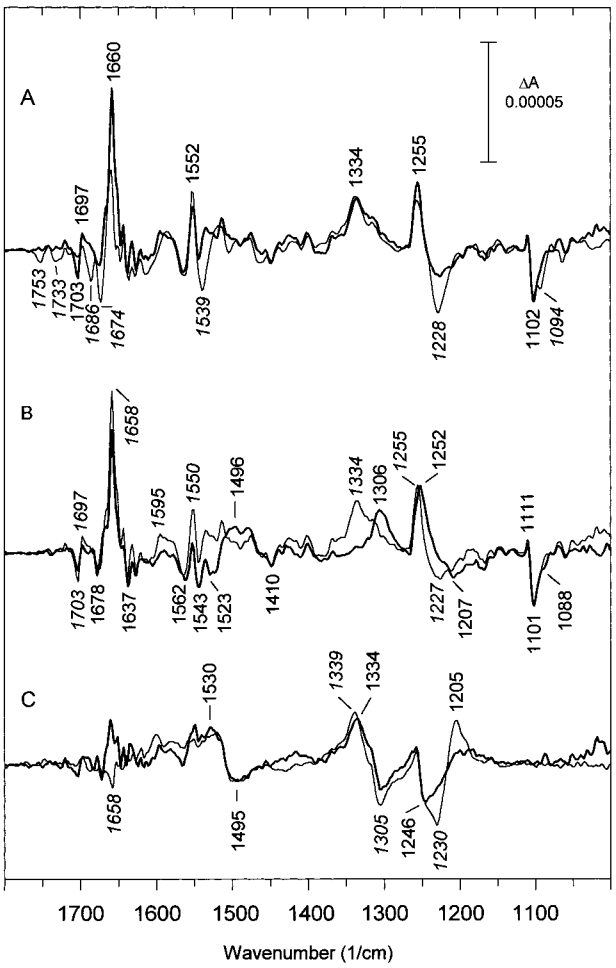

FIGURE 3: (A) Comparison of Fe^{2+}/Fe^{3+} spectra recorded at pH 7 in the presence (thick line) or in the absence (thin line) of *o*-phenanthroline. (B) Fe^{2+}/Fe^{3+} spectra recorded in the presence of *o*-phenanthroline and ^{12}C-bicarbonate (thin line) or ^{13}C-bicarbonate (thick line). (C) ^{12}C-*minus*-^{13}C-bicarbonate difference spectrum obtained from spectra in (B) (thick line), compared to that obtained with Fe^{2+}/Fe^{3+} spectra recorded in absence of *o*-phenanthroline (thin line). A total of ≈300 000 scans per spectrum, 4 °C.

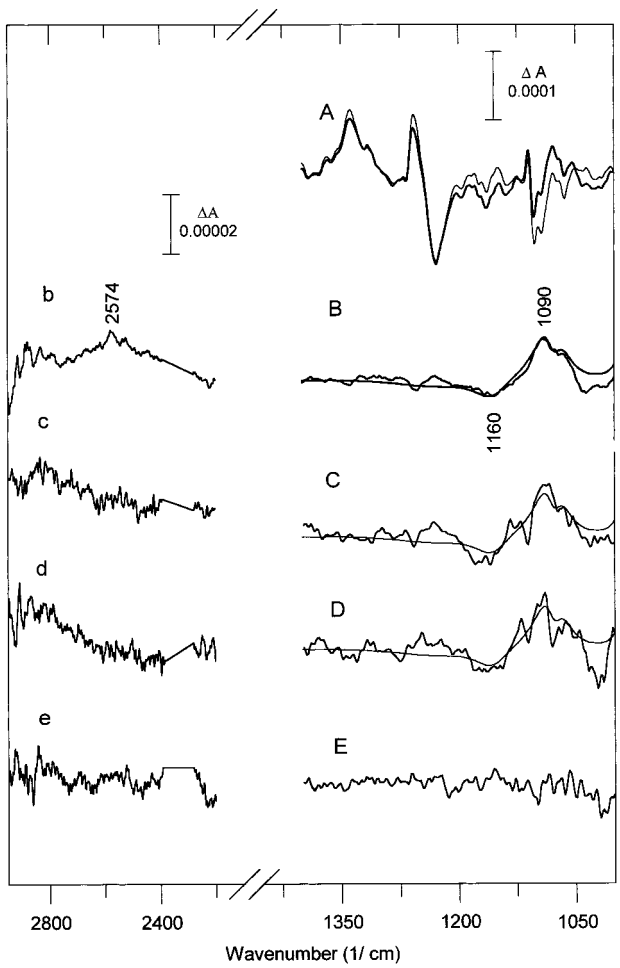

FIGURE 4: (A) Comparison of the 1400−1000 cm^{-1} region of the Fe^{2+}/Fe^{3+} FTIR spectra recorded with PS II in phosphate buffer (thick line) and Tris buffer (thin line) at pH 8. The spectra are adjusted to the same absorption of the ferrocyanide band at 2040 cm^{-1}. (B) Difference spectrum "phosphate-*minus*-Tris" (thick line) obtained by subtraction of spectra in (A), superimposed to the difference spectrum obtained with in vitro solutions of phosphate buffer at pH 8-*minus*-pH 6 (thin line). (C and D) "Phosphate-*minus*-MES" differences obtained with Fe^{2+}/Fe^{3+} spectra recorded at pH 6 in the presence of 50 mM glycolate or 50 mM lactate, respectively. (E) "Phosphate-*minus*-HEPES" difference obtained with Fe^{2+}/Fe^{3+} spectra recorded in the presence of *o*-phenanthroline at pH 7. The Fe^{2+}/Fe^{3+} spectra used to calculate the difference spectra of (C), (D), and (E) were normalized to the same absorption of the ferrocyanide band at 2040 cm^{-1} as spectra in (A). Spectra b−e: 2200−3000 cm^{-1} region of the Fe^{2+}/Fe^{3+} spectra recorded in the presence of bicarbonate, glycolate, lactate, and bicarbonate + *o*-phenanthroline, respectively; the spectra were normalized to the same absorption of the ferricyanide signal; for clarity, the region of CO_2 absorption has been deleted (2280−2400 cm^{-1}).

downshifts by ≈40 cm^{-1} upon ^{13}C labeling. The spectrum in Figure 3C, thick line, is actually close to that previously obtained without *o*-phenantroline with samples in ^2H_2O (*22*). The 1228 cm^{-1} band was previously interpreted as a coupling between the ν_s(CO) and δ(COH) modes, which no longer exists for deuterated bicarbonate. The broad band at 1246 cm^{-1} in Figure 3C, thick line, is also insensitive to $^2H/H$ exchange (not shown). Thus, in the presence of *o*-phenanthroline, either these two modes are not coupled or bicarbonate deprotonates upon iron oxidation. No signal sensitive to $^2H_2O/H_2O$ exchange could be assigned to the uncoupled δ-(COH) mode of bicarbonate, expected in the 1250−1000 cm^{-1} range. This signal may, however, be under the detection limit of the experiment.

The present IR data show that bicarbonate is still a ligand of the iron in the presence of *o*-phenanthroline, but with altered binding in the Fe^{3+} state. One clear effect of *o*-phenanthroline binding on the protein modes is shown by the absence of the negative band at 1094 cm^{-1} in the Fe^{2+}/Fe^{3+} spectrum of Figure 3A, thick line. Thus, the histidine ligand responsible for this band is perturbed upon *o*-phenanthroline binding. Also, signals at 1753 and 1733 cm^{-1} in the absorption region of CO ester groups or side chains of protonated glutamic or aspartic amino acids are totally absent in the Fe^{2+}/Fe^{3+} spectrum recorded in the presence of *o*-phenanthroline, as are negative signals at 1686 and 1539 cm^{-1}. Finally, the broad continuum band observed in the 2200−2800 cm^{-1} region of the Fe^{2+}/Fe^{3+} spectrum is totally absent in the spectrum recorded in the presence of *o*-phenanthroline, as shown in Figure 4e.

Measurement of Proton Release by PS II upon Iron Oxidation. Figure 4A compares the 1400−1000 cm^{-1} region of the Fe^{2+}/Fe^{3+} FTIR difference spectrum recorded at pH 8 in the presence of Tris (thin line) or phosphate buffer (thick

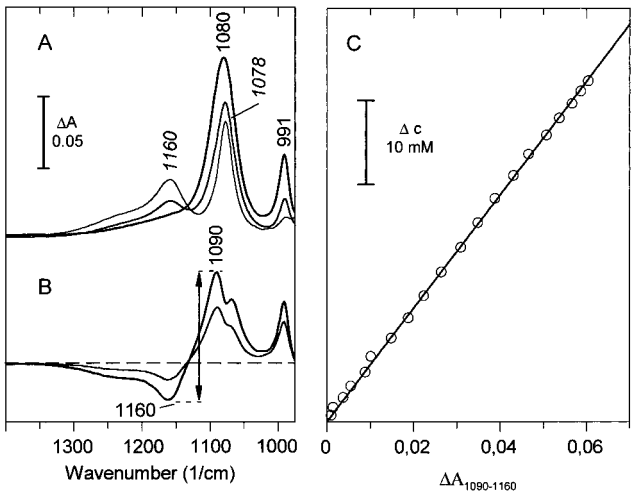

FIGURE 5: FTIR spectra of (A) 50 mM phosphate buffer at pH 6 (thin line), pH 7, and pH 8 (thick line). (B) Difference spectra pH 8-*minus*-pH 6 (thick line) and pH 8-*minus*-pH 7 (thin line). (C) Correlation between the absorption difference ΔA_P(1160−1090 cm^{-1}) and the concentration of $H_2PO_4^{2-}$.

line). The spectra were normalized to the same absorption of ferrocyanide at 2040 cm^{-1} (not shown). The spectra differ beyond 1200 cm^{-1} as shown by the difference denoted 'phosphate-*minus*-Tris' in Figure 4B (thick line). Two broad signals, negative at 1160 cm^{-1} and positive at 1090 cm^{-1}, are observed. The absorption spectra of 50 mM phosphate solutions at pH 8 (thick line), pH 7, and pH 6 (thin line) are shown in Figure 5A. The ν(P−O) modes of HPO_4^{2-} dominate at 1080 and 991 cm^{-1} in the spectrum recorded at pH 8, while $H_2PO_4^-$ ν(P═O) and ν(P−O) modes contribute at 1160 and 1078 cm^{-1} at pH 6 (*52*). The difference spectrum obtained with phosphate, pH 8-*minus*-pH 6, is shown in Figure 5B (thick line). It is very similar to the phosphate-*minus*-Tris spectrum observed for PS II in Figure 4B (thick line), and both spectra can be superimposed after appropriate scaling (Figure 4B, thin line). The signals observed at 1160 and 1090 cm^{-1} in Figure 4B are thus attributed to ν(P−O) stretching modes of phosphate buffer. They reflect proton uptake by the phosphate buffer upon non heme iron oxidation.

To quantify this proton uptake, difference spectra were computed between phosphate buffers at pH values ranging from pH 8 to 6, as illustrated in Figure 5B for pH 8-*minus*-pH 6 and pH 8-*minus*-pH 7 (thin line), and a correlation between the pH change and the absorption difference at 1090-*minus*-1160 cm^{-1}, ΔA_P(1090−1160 cm^{-1}), was established. Taking into account the different activity coefficients of $H_2PO_4^-$ and HPO_4^{2-}, the following relationship between pH and concentration of HPO_4^{2-} established by Cohn (*53*) was used:

$$\mathrm{pH} + \log\frac{1-X}{X} = \mathrm{p}K - \frac{1.5\sqrt{\mu}}{1+1.5\sqrt{\mu}} + K_s\mu$$

where X denotes the mole fraction of HPO_4^{2-}, μ the ionic strength, and K_s the so-called salting-out coefficient. We used the pK value of 7.2 given by Green for phosphate buffer (*54*) and a method of iterative approximations described by Mauk and Scott (*55*) to calculate this correlation. The linear relationship between ΔA_P(1090−1160 cm^{-1}) and concentration change of HPO_4^{2-} thus obtained is shown in Figure 5C. The data were fitted to a straight line with a slope $m_P = 686 \pm 5$ mM/au, which can be used to determine small concentration changes.

During the collection of the IR spectrum after illumination by a single laser flash of the PS II sample, no other redox site of PS II than the non heme iron contributes (*22*). Ferrocyanide acts as fast electron donor to the donor side of PS II (≤2 s), while the photoreduced non heme iron is slowly reoxidized by ferricyanide ($t_{1/2} \approx 20$ s at pH 8) (*22*). Therefore, the amount of ferrocyanide consumed after flash illumination, giving rise to the negative band at 2040 cm^{-1} in the Fe^{2+}/Fe^{3+} spectrum, is a direct measurement of the amount of PS II with photoreduced non heme iron (*22*). The correlation between the absorption change at 2040 cm^{-1} (ΔA_F) and the concentration change of ferrocyanide is given by the slope $m_F = 153 \pm 0.5$ mM/au (not shown). Knowing the coefficients m_P and m_F, the amount of protons released upon iron oxidation can be directly obtained from the absorption changes ΔA_F at 2040 cm^{-1} and ΔA_P(1090−1160 cm^{-1}) in the Fe^{2+}/Fe^{3+} spectrum. For PS II, $\Delta A_P = 7.6 \times 10^{-5}$ au and $\Delta A_F = 3.6 \times 10^{-4}$ au. The proton uptake by the phosphate buffer per non heme iron oxidized is then estimated to

$$\left(\frac{\Delta A_P}{\Delta A_F}\right)_{PSII}\left(\frac{m_P}{m_F}\right) = 0.95 \pm 0.05\ \mathrm{H^+/e^-}$$

The ≈10% error was obtained taking into account the noise level of the spectra. An analysis of Tris, HEPES, and MES buffers at different pH revealed that contributions of these buffers at 1160 and 1080−1090 cm^{-1} are negligible (not shown).

Figure 4C and Figure 4D show the difference spectra phosphate-*minus*-MES resulting from differences between spectra recorded at pH 6 with MES or phosphate in the presence of glycolate and lactate, respectively. In these spectra, phosphate IR modes are very similar to those observed in the presence of bicarbonate. It is concluded that equivalent proton release occurs upon iron oxidation in the presence of bicarbonate, glycolate, and lactate. In contrast, the phosphate-*minus*-HEPES difference spectrum obtained with spectra recorded with HEPES or phosphate buffer at pH 7 for PS II in the presence of *o*-phenanthroline is a straight line (Figure 4E). This spectrum demonstrates that *o*-phenanthroline binding prevents proton release upon iron oxidation in the presence of bicarbonate.

DISCUSSION

So far, the meaning of the specific properties of the non heme iron in PS II as compared to the bacterial RC is not really understood. What is the functional role of the exchangeable ligand bicarbonate? Is the low midpoint potential of the iron relevant for PS II function? What are the molecular mechanisms of the regulation by bicarbonate of the iron midpoint potential and how is it implicated in electron and proton transfer between Q_A and Q_B?

Answers to these questions require a better knowledge of the interactions of bicarbonate with its environment and with the Q_B binding pocket. Therefore, we used IR spectroscopy to analyze at the molecular level the structural perturbations

induced by bicarbonate exchange with glycolate, glyoxylate, and lactate, as well as those induced by *o*-phenanthroline binding. Proton release was quantified precisely and directly for these different conditions by a new method, comparing the absorption changes of phosphate buffer and ferrocyanide IR modes.

The IR data support an interaction between bicarbonate and the Q_B binding site through the regulation by bicarbonate of specific properties of the histidine D1−215 ligand of the iron and possibly of Q_B in a proximal binding site. The influence of *o*-phenanthroline binding on the proton release observed upon iron oxidation in the presence of bicarbonate also points to the specific implication of bicarbonate in a proton-transfer chain toward the Q_B pocket.

Bicarbonate Exchange with Other Anions. Bicarbonate replacement by small carboxylate anions has been studied in detail by Y. Deligiannakis, V. Petrouleas, and B. Diner (*34*, *43*). According to EPR data, bicarbonate substitution by these anions alters both $E_m(Fe^{3+}/Fe^{2+})$ and its pH dependence. This was interpreted as the change in pK^R and pK^O (where O and R are iron-oxidized and -reduced, respectively) of the protonatable group(s) which determine(s) the E_m of the iron couple (*34*). This regulation correlates also with the different *g* value of the Q_A^-−Fe^{2+} EPR spectrum observed at high or low pH and in the presence of lactate versus formate (*34*). Since bicarbonate depletion or its exchange also alters electron transfer between Q_A^- and Q_B (*26*−*28*, *43*), the same residue(s) was (were) proposed to be implicated in the protonation reactions accompanying these electron-transfer reactions (*43*). The present study shows that more complex mechanisms accompany bicarbonate exchange.

The IR frequencies of lactate strongly indicate that lactate displaces bicarbonate by direct binding to the iron as a bidentate ligand, bound through one carboxylate oxygen and the hydroxyl group both in the Fe^{2+} and in the Fe^{3+} states. The structural analogy between lactate and glycolate and the similarity of both the Fe^{3+} EPR (*34*) and Fe^{2+}/Fe^{3+} FTIR spectra recorded in the presence of these two anions suggest that they adopt the same mode of binding to the iron. We previously concluded from IR data that bicarbonate is a bidentate ligand of Fe^{2+} and a monodentate ligand of Fe^{3+} (*22*). The lower midpoint potential of the iron couple observed in the presence of lactate (−120 mV at pH 6) could be explained in part by a stabilization of the Fe^{3+} state through the additional ligand provided by lactate compared to bicarbonate. However, in the presence of bicarbonate, a sixth ligand provided by the protein or by a water molecule cannot be excluded in the Fe^{3+} state.

The direct effect on $E_m(Fe^{3+}/Fe^{2+})$ of monodentate or bidentate binding of the anions is accompanied by effects of glycolate, glyoxylate, and lactate on the protein around the iron. One common observation in the Fe^{2+}/Fe^{3+} spectra recorded with the three anions is the perturbation of the ν(C−N) mode of (at least) one histidine ligand of the iron. We previously assigned the IR signals at 1111/1102 and 1094 cm^{-1} in the Fe^{2+}/Fe^{3+} spectrum to histidine ligands of the iron, on the basis of their sensitivity to ^{15}N labeling and by comparison with IR data of iron protoporphyrin IX−imidazole model compounds (*22*, *56*). These assignments are supported by results obtained recently by Noguchi and coworkers (*57*, *58*). They reported a negative band at 1100 cm^{-1} sensitive to His ^{15}N labeling in the Fe^{2+}/Fe^{3+} spectrum recorded at pH 5.5 with PS II cores of *Synechocystis*. A signal at 1109/1102 cm^{-1} in the Q_A^-/Q_A FTIR spectrum was assigned to D2His215, a putative iron ligand proposed to hydrogen bond to Q_A (*58*). Part of the 1111/1102 cm^{-1} signal of the Fe^{2+}/Fe^{3+} spectrum is probably contributed by this histidine. Also, Noguchi et al. showed that the ν(C−N) IR mode of neutral HisNπH absorbs at 1106 cm^{-1} and is almost insensitive to $^2H/^1H$ exchange, while for HisNτH this mode absorbs at 1090 cm^{-1} and is upshifted by +6 cm^{-1} upon $^2H/^1H$ exchange (*57*). Thus, the signal at 1111/1102 cm^{-1} in the Fe^{2+}/Fe^{3+} spectrum, insensitive to $^2H/^1H$ exchange, corresponds to neutral histidine(s) bound to the iron at the Nτ imidazole nitrogen, as expected from comparison with bacterial RC (*2*, *4*−*7*, *9*−*16*). The signal at 1094 cm^{-1}, insensitive to $^2H/^1H$ exchange, has a frequency too low to account for the ν(C−N) mode of neutral HisNπH. The ν(C−N) mode of the ligand methyl imidazolate in iron protoporphyrin IX−methylimidazole complexes has a lower frequency than methylimidazole (−4 cm^{-1}) and a larger absorption coefficient (*56*). In solution, His^- also absorbs at a frequency lower than HisNπH (−5 cm^{-1})(*57*). These data lead to the assignment of the band at 1094 cm^{-1} in the Fe^{2+}/Fe^{3+} spectrum to the ν(C−N) mode of a histidinate ligand in the Fe^{3+} state. This signal observed in Fe^{2+}/Fe^{3+} spectra recorded at pH 6−8 (*22*, *41*, and probably *40*) was not present in spectra recorded at 200 K and pH 5.5 (*40*, *57*). The absence of the IR band of the His^- ligand upon replacement of bicarbonate by glycolate, glyoxylate, and lactate suggests a specific regulation of the His pK_a by bicarbonate. It is therefore likely that this histidine ligand is the group responsible for the pH-dependent midpoint potential of the iron in the presence of bicarbonate. At present, we cannot totally exclude, however, a contribution of the arginine or lysine ν(C−N) side chain mode at this frequency.

In the Fe^{2+}/Fe^{3+} spectrum recorded in the presence of bicarbonate, a broad positive continuum is observed at 2200−2800 cm^{-1} (Figure 4b). The continuum band correlates with the presence of bicarbonate and of the His^- ligand in the Fe^{3+} state, since it is absent in the Fe^{2+}/Fe^{3+} spectra recorded with PS II samples with glycolate and lactate (Figure 4c,d) and in an Fe^{2+}/Fe^{3+} spectrum recorded with *Synechocystis* PS II cores, where the band at 1094 cm^{-1} is also lacking (*57*). Similar broad continuum bands in this spectral region or at lower frequencies (2300−1800 cm^{-1}) were reported in FTIR spectra recorded with bacterial RC, PS II, and bacteriorhodopsin (*50*, *57*, *59*, *60*). Systematic studies have shown that the polarizability of a delocalized proton in a hydrogen-bonded network causes such broad continuum absorbencies (*50*, *51*, *61*). In bacteriorhodopsin, changes in IR continuum bands have been observed during proton pumping events which could not be associated with localized changes at aspartic or glutamic side chains. These changes were interpreted as fast proton transfer on the uptake pathway via a complex hydrogen-bonded network of protons donated by the bulk phase or internal H_2O/H_3O^+, which could be connected to the network (*59*, *60*). Internal water molecules within a potential proton channel were also evidenced by the structure of bacteriorhodopsin (*62*). The positive continuum bands associated with Q_A and Q_B reduction in bacterial RC and similar to signals observed with hydronium ions have been assigned to a net proton uptake within a large network of polarizable hydrogen bonds (*48*, *50*, *51*). The

continuum observed in the Fe^{2+}/Fe^{3+} spectrum in the presence of bicarbonate presents the characteristics of an increase in delocalized proton(s) within a similar network of polarized hydrogen bonds upon iron reduction.

Effect of Iron Oxidation/Reduction on the Q_B Pocket. Bicarbonate is required for the interaction between the iron environment and this network of hydrogen-bonded molecules. The IR continuum could sense an interaction between the iron and the Q_B binding site through bicarbonate and the histidine. Indeed, the Fe^{2+}/Fe^{3+} FTIR spectrum recorded with PS II in the presence of *o*-phenanthroline also lacks both the broad IR continuum and the 1094 cm^{-1} band. The absence of the 1094 cm^{-1} signal strongly suggests that it is due to D1His215, homologous to the LHis190 ligand of the iron and of Q_B (proximal Q_B binding site) in the bacterial RC (*5, 6, 13, 18*). *o*-Phenanthroline binding to D1His215 would modify the pK^O of this ligand and hinder its deprotonation upon iron oxidation.

The binding affinity of DCMU, *o*-phenanthroline, and atrazine for the Q_B pocket is strongly affected by iron oxidation (*29, 38, 63, 64*). Positive shifts of the iron midpoint potential consistent with those predicted from the altered dissociation constants were observed by EPR for DCMU and atrazine (*38*). For *o*-phenanthroline, an $E_m(Fe^{3+}/Fe^{2+})$ increase by 60 mV at pH 7 is derived from the altered binding constants (*38*), which might result from the loss of D1His215 deprotonation and subsequent proton release during iron oxidation.

In the bacterial RC, *o*-phenanthroline binds with its two nitrogens sharing a hydrogen bond with the imidazole NτH group of LHis190 (*2, 4, 65*). Atrazine binds at the opposite side of the Q_B pocket interacting with LHis190 through a water molecule (*66*), in a way similar to terbutryn (*2*) and to Q_B bound at the distal site (*13*). Homologous point mutations leading to atrazine resistance in PS II and bacterial RC suggest a similar binding in both photosystems, i.e., without direct interaction with D1His215 in PS II (*8*). Of these herbicides, only *o*-phenanthroline modifies the Fe^{3+} EPR spectrum in PS II, with a large resonance observed at $g = 6$ which suggests axial coordination of the iron (*17, 32, 37, 38*). The IR data support the attribution of the $g = 6$ Fe^{3+} EPR signal to centers with Q_B or *o*-phenanthroline directly hydrogen bonded to D1His215 (*36*), while the $g = 8$ form would correspond to PS II centers with an empty Q_B pocket or with triazine-like herbicides.

Two water molecules interact with LHis190 in the empty Q_B pocket of *Rps. viridis* or in RC with bound triazines (*66*). They also interact with water molecules of a hydrogen bond network from the cytoplasm to the Q_B site (*12, 66, 67*) roughly similar to that first observed for *Rb. sphaeroides* (*9, 11, 13*). Structural changes at LHis190 are susceptible to perturb such a hydrogen bond network. In PS II, the broad continuum observed in the Fe^{2+}/Fe^{3+} spectrum which is suppressed upon *o*-phenanthroline binding could result from similar interactions between the iron ligand D1His215 and a hydrogen bond network at the Q_B pocket. As discussed above, this interaction depends on the presence of bicarbonate.

Proton Release by PS II upon Iron Oxidation. Phosphate buffer signals have been observed in FTIR difference spectra of electrochemically or photochemically generated reactions in proteins involved in electron and proton transfer (*68*−*70*). These buffer signals are associated with proton release/uptake by the protein upon oxidation/reduction of cofactors. In PS II, proton release at the protein surface upon $Tyr_D^{\bullet}$ formation was thus reported *(69)*. Quantitation of proton release requires, however, the accurate determination of the number of redox centers involved in the redox reaction. To obtain an accurate quantification of proton release per PS II centers, we used the ferrocyanide IR signal at 2040 cm^{-1} as 'internal counter' of the amount of non heme iron photoreduced after flash illumination. Direct comparison of ferrocyanide and phosphate IR signals in the FTIR spectrum avoids the determination of sample thickness or RC concentration, both of which are difficult to estimate for an IR sample of PS II enriched membranes.

With bicarbonate as a ligand and in the pH range 6−8, the proton release by PS II measured upon non heme iron oxidation is close to 1. The observed phosphate buffer signals are a direct monitor of the −60 mV/pH unit dependence of the iron midpoint potential. This proton release is totally suppressed upon *o*-phenanthroline binding, supporting that it is connected to the Q_B pocket. Proton release of about 1 is also observed in the presence of the carboxylate anions lactate or glycolate at pH 6. These data cannot be reconciled with the absence of pH dependence of the iron midpoint potential reported for lactate but may agree with the pH effect observed for glycolate by EPR spectroscopy between pH 6 and 7 (*34*). This direct proton release measurement which involves IR modes with high extinction coefficients may be more accurate than the comparison of Fe^{3+} EPR signals recorded with different ferri/ferrocyanide solutions in different samples. This result shows that the alteration of the iron midpoint potential upon bicarbonate replacement by other anions cannot be modeled only by the change in pK_a of a group (possibly D1His215). In the presence of both glycolate and *o*-phenanthroline, a similar proton release was measured (data not shown). Although *o*-phenanthroline binding may be modified in the presence of glycolate, this observation together with the absence of the IR signal at 1094 cm^{-1} and of the continuum at 2400−2800 cm^{-1} in the presence of the anions suggests that the proton release in the presence of glycolate does not involve D1His215 nor protein group(s) located at the Q_B site.

In conclusion, the present work demonstrates specific interactions of bicarbonate with the Q_B pocket of PS II. In particular, the data strongly indicate interaction of bicarbonate with the non heme iron ligand D1His215 of the Q_B pocket either directly or via a hydrogen bond network. Identification of amino acid side chains implicated in the hydrogen bond network around bicarbonate would need the investigation of site-directed mutants and/or PS II with specifically labeled amino acid side chains. We have also developed an accurate method to quantify proton release by the protein upon non heme iron oxidation in buffered conditions. This method can be used to measure proton release/uptake of other transitions in PS II as well as in other biological systems.

ACKNOWLEDGMENT

Y. Deligiannakis and V. Petrouleas are gratefully acknowledged for discussions on the experimental aspects of bicarbonate exchange by other ions and also for discussions on the EPR and Mössbauer results. We also thank A. Boussac, J. Breton, J. Lavergne, and A. Verméglio for useful discussions and critical reading of the manuscript.

REFERENCES

1. Diner, B. A., Petrouleas, V., and Vendolowski, J. J. (1991) *Physiol. Plant. 81*, 423−436.
2. Michel, H., Epp, O., and Deisenhofer, J. (1986) *EMBO J. 5*, 2445−2451.
3. Trebst, A. (1986) *Z. Naturforsch. 41C*, 240−245.
4. Allen, J. P., Feher, G., Yeates, T. O., Komiya, H., and Rees, D. C. (1987) *Proc. Natl. Acad. Sci. U.S.A. 84*, 6162−6166.
5. Michel, H., and Deisenhofer, J. (1988) *Biochemistry 27*, 1−7.
6. Deisenhofer, J., and Michel, H. (1989) *EMBO J. 8*, 2149−2169.
7. Ruffle, S. V., Donnelly, D., Blundel, T. L., and Nugent, J. H. A. (1992) *Photosynth. Res. 34*, 287−300.
8. Egner, U., Hoyer, G.-A., and Saenger, W. (1993) *Biochim. Biophys. Acta 1142*, 106−114.
9. Ermler, U., Fritzsch, G., Buchanan, S. K., and Michel, H. (1994) *Structure 2*, 925−936.
10. Arnoux, B., Gaucher, J. F., Ducruix, A., and Reiss-Husson, F. (1995) *Acta Crystallogr., Sect. D 51*, 368.
11. Lancaster, C. R. D., and Michel, H. (1996) *Photosynth. Res. 48*, 65−74.
12. Lancaster, C. R. D., and Michel, H. (1997) *Structure 5*, 1339−1359.
13. Stowell, M. H. B., McPhillips, T. M., Rees, D. C., Soltis, S. M., Albresch, E., and Feher, G. (1997) *Science 276*, 812−816.
14. Svensson, B. (1995) Ph.D. Thesis, Stockholm University, Stockholm, Sweden.
15. Svensson, B., Etchebest, C., Tuffery, P., Kan, van P., Smith, J., and Styring, S. (1996) *Biochemistry 35*, 14486−14502.
16. Xiong, J., Subramaniam, S., and Govindjee (1996) *Protein Sci. 5*, 2054−2073
17. Diner, B. A., and Petrouleas, V. (1987) *Biochim. Biophys. Acta 895*, 107−125.
18. Allen, J. P., Feher, G., Yeates, T. O., Komiya, H., and Rees, D. C. (1988) *Proc. Natl. Acad. Sci. U.S.A. 85*, 8487−8491.
19. Diner, B. A., and Petrouleas, V. (1990) *Biochim. Biophys. Acta 1015*, 141−149.
20. Petrouleas, V., and Diner, B. A. (1990) *Biochim. Biophys. Acta 1015*, 131−140.
21. Koulougliotis, D., Kostopoulos, T., Petrouleas, V., and Diner, B. A. (1993*) Biochim. Biophys. Acta 1141*, 275−282.
22. Hienerwadel, R., and Berthomieu, C. (1995) *Biochemistry 34*, 16288−16297.
23. Deligiannakis, Y., Tsekos, N., Petrouleas, V., and Diner, B. A. (1992) *Biochim. Biophys. Acta 1140*, 260−270
24. Blubaugh, D., and Govindjee (1988) *Photosynth. Res. 19*, 85−128.
25. Govindjee and van Rensen, J. J. S. (1993) in *The Photosynthetic Reaction Center* (Deisenhofer, J., and Norris, J., Eds.) Vol. I, pp 357−389, Academic Press, San Diego, CA.
26. Van Rensen, J. J. S., Tonk, W. J. M., and De Bruijn, S. M. (1988) *FEBS Lett. 226*, 347−351.
27. Stemler, A., and Murphy, J. B. (1985) *Plant Physiol. 77*, 974−977.
28. Eaton-Rye, J. J., and Govindjee (1988) *Biochim. Biophys. Acta 935*, 237−257.
29. Wraigth, C. A. (1985) *Biochim. Biophys. Acta 809*, 320−330.
30. Vermaas, W., Van Rensen, J. J. S., and Govindjee (1982) *Biochim. Biophys. Acta 681*, 242−247.
31. Ikegami, I., and Katoh, S. (1973) *Plant Cell Physiol. 14*, 829−836.
32. Bowes, J. M., Crofts, A. R., and Itoh, S. (1979) *Biochim. Biophys. Acta 547*, 320−335.
33. Petrouleas, V., and Diner, B. A. (1986) *Biochim. Biophys Acta 849*, 264−275
34. Deligiannakis, Y., Petrouleas, V., and Diner, B. A. (1994) *Biochim. Biophys. Acta 1188*, 260−270.
35. Hienerwadel, R., and Berthomieu, C. (1995) in *Photosynthesis: from Light to Biosphere* (Mathis, P., Ed.) Vol. I, pp 743−746, Kluwer Academic Publishers, Dordrecht, The Netherlands.
36. Petrouleas, V., and Diner, B. A. (1987) *Biochim. Biophys. Acta 893*, 126−137.
37. Itoh, S., Tang, X.-S., and Satoh, K. (1986) *FEBS Lett. 205*, 275−281.
38. Diner, B. A., and Petrouleas, V. (1987) *Biochim. Biophys. Acta 893*, 138−148.
39. Hienerwadel, H., Boussac, A., and Berthomieu, C. (1993) in *Fifth International Conference on the Spectroscopy of Biological Molecules* (Theophanides, T., Anastassopoulou, J., and Fotopoulos, N., Eds.) pp 317−318, Kluwer Academic Publisher, Dordrecht, The Netherlands.
40. Noguchi, T., and Inoue, N. (1995) *J. Biochem. 118*, 9−12.
41. Chu, H.-A., Hillier, W., Law, N. A., Sackett, H., Haymond, S., and Babcock, G. T. (2000) *Biochim. Biophys. Acta 1459*, 528−532.
42. Petrouleas, V., Sanakis, Y., Deligiannakis, Y., and Diner, B. A. (1992) in *Research in Photosynthesis* (Murata, Ed.) Vol. II, pp 119−122, Kluwer Academic Publishers, Dordrecht, The Netherlands.
43. Petrouleas, V., Deligiannakis, Y., and Diner, B. A. (1994) *Biochim. Biophys. Acta 1188*, 271−277.
44. Cassanas, G., Morssli, M., Fabrègue, E., and Bardet, L. (1991) *J. Raman Spectrosc. 22*, 409−413.
45. Goulden, J. D. S. (1960) *Spectrochim. Acta 16*, 715−720.
46. Deacon, G. B., and Phillips, R. J. (1980) *Coord. Chem. Rev. 33*, 227−250.
47. Larsson, R. (1965) *Acta Chem. Scand. 19*, 783−790.
48. Nakamoto, K., McCarthy, P. J., and Miniatas, B. (1965) *Spectrochim. Acta 21*, 379−388.
49. Breton, J., Nabedryk, E., Allen, J. P., and Williams, J. A. C. (1997) *Biochemistry 36*, 4515−4525.
50. Breton, J., and Nabedryk, E. (1998) *Photosynth. Res. 55*, 301−307.
51. Zundel, G. (1988) *J. Mol. Struct. 177*, 43−68.
52. Socrates, G. (1994) in *Infrared Characteristic Group Frequencies, Table and Charts*, Second ed., John Wiley & Sons Ltd., Chichester, England.
53. Cohn, E. J. (1927) *J. Am. Chem. Soc. 49*, 173−193.
54. Green, A. A. (1933) *J. Am. Chem. Soc. 55*, 2331−2337.
55. Mauk, A. G., and Scott, R. A. (1981) *Comput. Chem. 5*, 67−69.
56. Berthomieu, C., Boussac, A., Mäntele, W., Breton, J., and Nabedryk, E. (1992) *Biochemistry 31*, 11460−11471.
57. Noguchi, T., Inoue, Y., and Tang, X.-S. (1999) *Biochemistry 38*, 10187−10195.
58. Noguchi, T., Inoue, Y., and Tang, X.-S. (1999) *Biochemistry 38*, 399−403.
59. Le Coutre, J., Tittor, J., Oesterhelt, D., and Gerwert, K. (1995) *Proc. Natl. Acad. Sci. U.S.A. 92*, 4962−4966.
60. Rammelsberg, R., Huhn, G., Lübben, M., and Gerwert, K. (1998) *Biochemistry 37*, 5001−5009.
61. Zundel, G. (1992) *Trends Phys. Chem. 3*, 129−156.
62. Pebay-Peroula, E., Rummel, G., Rosenbusch, J. P., and Landau, E. M. (1997) *Science 77*, 1676−1681.
63. Renger, G., Hagemann, R., and Fromme, P. (1986) *FEBS Lett. 203*, 210−214.
64. Diner, B. A., and Petrouleas, V. (1987) *Biochim. Biophys. Acta 895*, 107−125.
65. Chang, C. H., Tiede, D., Tang, J., Smith, U., Norris, J., and Schiffer, M. (1986) *FEBS Lett. 205*, 82−86.
66. Lancaster, C. R. D., and Michel, H. (1999) *J. Mol. Biol. 286*, 883−898.
67. Lancaster, C. R. D. (1998) *Biochim. Biophys. Acta 1365*, 143−150.
68. Hellwig, P., Rost, B., Kaiser, U., Ostermeier, C., Michel, H., and Mäntele, W. (1996) *FEBS Lett. 385*, 53−57.
69. Hienerwadel, R., Boussac, A., Breton, J., and Berthomieu, C. (1996) *Biochemistry 35*, 15447−15460.
70. Baymann, F., Robertson, D. E., Dutton, P. L., and Mäntele, W. (1999) *Biochemistry 38*, 13188−13199.

BI002236L